# Semantically-Aware Attentive Neural Embeddings for Long-Term 2D Visual Localization

Zachary Seymour

Karan Sikka

SRI International 201 Washington Road Princeton, NJ

#### Abstract

We present an a 2D image-based loc Compared to appear end deep attention-embeddings for 2D-and modality-specifi image regions. We challenging localization We present an approach that combines appearance and semantic information for 2D image-based localization (2D-VL) across large perceptual changes and time lags. Compared to appearance features, the semantic layout of a scene is generally more invariant to appearance variations. We use this intuition and propose a novel end-toend deep attention-based framework that utilizes multimodal cues to generate robust embeddings for 2D-VL. The proposed attention module predicts a shared channel attention and modality-specific spatial attentions to guide the embeddings to focus on more reliable image regions. We evaluate our model against state-of-the-art (SOTA) methods on three challenging localization datasets. We report an average (absolute) improvement of 19% over current SOTA for 2D-VL. Furthermore, we present an extensive study demonstrating the contribution of each component of our model, showing 8-15% and 4% improvement from adding semantic information and our proposed attention module. We finally show the predicted attention maps to offer useful insights into our model.

#### Introduction 1

Visual localization (VL) is the problem of estimating the precise location of a captured image and is crucial to applications in autonomous navigation [4, 22, 53, 53, 53, 53, 42]. Here, we target the problem of *long-term VL* [ , , , , , , , , , , , ] in real-world environments, which is required to operate under (1) extreme perceptual changes such as weather and illumination, and (2) dynamic scene changes and occlusions such as moving vehicles. We also evaluate this task to focus on a key requirement of long-term VL, which is to localize within a narrow radius of <10m instead of 25m- the localization radius for evaluating the related task of place recognition  $[\mathbf{N}, \mathbf{Z}]$ .

<sup>© 2019.</sup> The copyright of this document resides with its authors. It may be distributed unchanged freely in print or electronic forms.

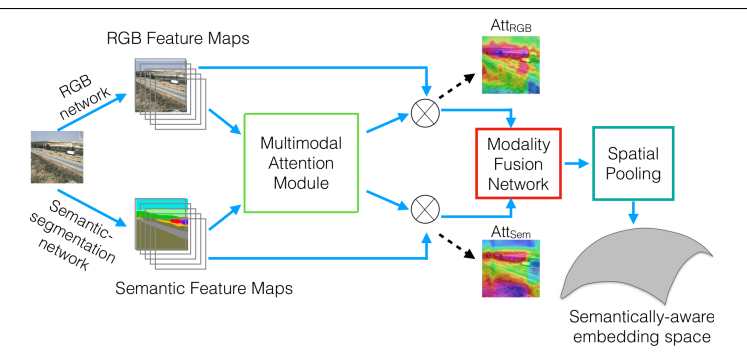


Figure 1: We show a high-level overview (top) of our approach (SAANE) that learns to effectively combine appearance and semantic information with modality-specific spatial attention to compute semantically-aware feature embeddings in the presence of severe changes in viewing conditions.

Prior works on VL generally utilize two broad classes of methods: 3D structure-based localization (3D-VL) and 2D image-based localization (2D-VL) [124], [155], both of which utilize local or global low-level appearance descriptors. 3D-VL methods typically associate a local descriptor with each point in a 3D model of the scene [125], [151], while 2D-VL methods extract a holistic descriptor or multiple local descriptors for query-based matching [151], [152]. A primary drawback with methods using low-level features is that they are not robust to changes in viewing conditions [152], [153]; while 3D models are less scalable and present greater computational complexity. To this end, we focus on improving 2D-VL methods specifically for operating under severe changes in viewing conditions in large-scale urban environments and over large time lags [153].

Recently 2D-VL methods have used deep convolutional neural networks (DCNN) based frameworks that learn to generate view-invariant image representations (or embeddings) [N, 23, 53]. Despite advancing the state-of-the-art, DCNN still suffer from two key issues in long-term VL. First, due to the reliance on low or mid-level appearance features, DCNN methods suffer a loss in accuracy for large changes in viewing conditions [153, 165]. Second, since DCNN methods extract holistic representations from an entire image without any explicit understanding of scene composition, the resulting image representation is degraded by non-discriminative visual elements (vehicles) [153, 165]. To alleviate these issues, we propose a novel DCNN framework to improve the robustness of learned visual embeddings by incorporating (i) high-level semantic information inside the neural network, and (ii) an attention-based framework that uses both appearance and semantic information to guide the model to focus on informative and stable image regions.

Our method, referred to as Semantically-Aware Attentive Neural Embeddings (SAANE) (see Figure 1), is an end-to-end trainable deep neural network, that effectively combines semantic 1 and mid-level appearance features with spatial attention to learn semantically-aware embeddings. The design of SAANE is inspired by recent advances in deep multimodal and attention guided learning [II, IZ, EI], EI] and is composed of three key modules: (i) the *modality fusion module:* to fuse information from the two modalities, (ii) the *multimodal attention module:* to use the fused representation to predict a shared channel attention and separate modality-specific spatial attentions, and (iii) the *spatial pooling module:* to pool

<sup>&</sup>lt;sup>1</sup>By *semantic* we refer to representations that provide high-level information about the input; *e.g.*, per-pixel depth or semantic segmentation maps.

the attended multimodal features to generate embeddings, which are then used to retrieve matches for a query image. We use convolutional feature maps from models pre-trained for image classification and semantic segmentation as appearance and semantic representations respectively. Our model is trained end-to-end by using a ranking based objective.

The key motivation behind our approach is that compared to low/mid-level appearance descriptors, the spatial layout of semantic classes in the image yields scene descriptions that have a higher invariance to large changes in viewing conditions for long-term VL. The semantic understanding of the image content along with spatial attention helps to determine which regions of the scene may be unreliable for localization across large time scales. A key advantage of SAANE over prior works, that have attempted to improve the robusness of low-level features, is that it offers a principled end-to-end module to learn semantically-aware representations with spatial attention- guided by multimodal features.

The key contributions of this paper are as follows:

- 1. We incorporate higher-level semantic information along with commonly-used mid-level appearance features to enhance the quality of the *learned* image embeddings for visual localization under large appearance changes.
- 2. We propose an attention-based neural module to allow the model to focus on stable and discriminative regions. To the best of our knowledge, ours is the first work to propose a DCNN-based pipeline that combines multimodal representations (appearance and semantic), with spatial attention for visual localization.
- 3. We perform extensive ablation studies across three datasets to show the contributions of each part of our model. We particularly investigate and establish the necessity of the proposed separable spatial with shared channel attention for current problem.

#### 2 Related Work

Methods for image-based visual localization generally fall into two classes: 3D structure-based localization (3D-VL) [13, 141, 151, 152] and 2D image-based localization (2D-VL) [18, 141, 142, 143, 143, 143] and 2D image-based localization (2D-VL) [18, 142, 143, 143]. 3D-VL methods create a 3D model of the scene by either using Structure-From-Motion (SfM) or associating local patches to 3D point clouds. On the other hand, 2D-VL methods formulate visual localization as an image retrieval problem by matching a query image with geo-tagged database images for approximate localization. In this paper we focus on improving 2D-VL methods in large-scale scenes, which can then be used in combination with 3D methods for more precise localization as shown in [141].

Most initial works for visual localization relied on matching Bag of Visual Word (BoVW)-type features [1, 22] or using global image descriptors in addition to sequential search [66]. Building on the success of deep convolutional neural networks (DCNN) in other areas [21], 22], recent works have extensively demonstrated the effectiveness of off-the-shelf DCNN features for visual place recognition and VL [111, 221, 511]. Several works have also focused on improving feature pooling methods for off-the-shelf features [1, 512] or those learned in end-to-end pipelines [18, 513].

In general, (deep) learned global descriptors are more robust than hand-crafted features but are still susceptible to perceptual aliasing from repeated patterns such as road markings and buildings that introduce indistinguishable global matches; *i.e.*, only specific, meaningful regions are useful for localization [ $\square$ ,  $\square$ ]. In prior works, the contribution of combining

mid-level image features with higher-level semantic information has been entangled with the addition of 3D information [11], 126]. Semantics were also used to focus on manually-selected regions [123] or to enhance off-the-shelf appearance features [12], 120]. Our method's novel multimodal attention module learns not only to combine features across modalities but also to focus on the most stable regions by discovering region types in a data-driven fashion.

We also situate our work within the space of making image features semantically-grounded and more robust to appearance changes. A typical approach to matching image features across large perceptual changes is to learn a transformation from one type of appearance to another—such as across seasons [5] or across different times of day [6], 5]—or to train a DCNN for appearance invariance using paired images [6], 5]. Our method seeks to integrate this innovation with stable semantic scene features to further improve the invariance of these features.

Our work is also related to recent works on combining vision and language for the Visual Question Answering (VQA) task [3]. The underlying fusion networks vary from pooling methods such as sum/bilinear pooling [3] to more complex attention based methods [4], 32, 33]. Although the proposed multimodal attenion module is motivated by these works, it is both different and better suited to the requirements of the long-term VL task, which is fundamentally different from the VQA task. For example, the appearance and semantic modalities in VL are more closely-aligned as compared to vision and language in VQA, due to which additional blocks are required for aligning the modalities prior to fusion.

# 3 Approach: SAANE

We now describe our approach, referred to as **SAANE** (Semantically-Aware Attentive Neural Embeddings), in detail. Our model passes an input RGB through two DCNNs pre-trained for image classification and semantic segmentation to obtain mid-level appearance features (denoted as  $App_{\text{mid}}$ ) and high-level semantic features (denoted as  $Sem_{\text{high}}$ ) respectively. We denote feature maps from layer l of the image-classification and semantic-segmentation CNNs as  $\mathbf{F}_l^A \in \mathbb{R}^{C_A \times H \times W}$  and  $\mathbf{F}_l^S \in \mathbb{R}^{C_S \times H \times W}$  respectively, where  $C_A$  and  $C_S$  are the number of channels. We drop the notation l in the rest of the paper for brevity. We work in a supervised setting with a database of geo-tagged images captured under different viewing conditions.

SAANE is an end-to-end trainable DCNN that learns to generate robust image embeddings that, in addition to being invariant to changes in viewing conditions, are aware of semantic composition of the scene and focus explicitly on informative visual elements due to the use of spatial attention. Our model (Figure 1) consists of three NN-based modules: (i) the modality fusion module, (ii) the multimodal attention (MM-Att) module, and (iii) the spatial pooling module. SAANE operates by first transforming and fusing features from the appearance and the semantic input streams by using the modality fusion module. The output is a semanticallyinformed multimodal representation of input, which is then used to estimate per-modality spatial attentions using the proposed MM-Att module. We encourage sharing of information between the two modalities by building upon a prior work for unimodal attention [\sum\_] and computing a shared channel attention which is then used to generate separate spatial attentions as described below. The output from this module is used to refine the feature maps from both modalities, which are then fused together with another modality fusion module. Finally, we use a spatial pooling to output the embeddings. We train our model in an end-to-end fashion to learn each of these modules for visual localization. We now describe these modules along with the loss function and the training procedure.

**Modality Fusion Module.** The modality fusion module aligns the feature maps— $App_{\text{mid}}$  and  $Sem_{\text{high}}$ —by first projecting them in a common space and then adding them together [2, 51]. We use  $1 \times 1$  convolutions, denoted by  $\mathbf{W}_A^1 \in \mathbb{R}^{C \times C_A \times 1 \times 1}$  and  $\mathbf{W}_S^1 \in \mathbb{R}^{C \times C_S \times 1 \times 1}$  for the appearance and semantic streams respectively, to project the feature maps in a C-dimensional common space.

$$\mathbf{F}^{M} = \mathbf{W}_{A}^{1} \circledast \mathbf{F}^{A} + \mathbf{W}_{S}^{1} \circledast \mathbf{F}^{S}$$
$$= \mathbf{F}_{A}^{M} + \mathbf{F}_{S}^{M}, \tag{1}$$

where  $\mathbf{F}^M$  is the fused multimodal representation of the image,  $F_A^M$  and  $F_S^M$  are the aligned features maps from  $App_{\mathrm{mid}}$  and  $Sem_{\mathrm{high}}$  respectively, and  $\circledast$  is the convolutional operator. The output is a semantically-informed multimodal representation of the input and is used as input to both MM-Att and later to the spatial pooling module. Although recent methods have used sophisticated pooling approaches [ $\square$ ], we opted for projected sum pooling, as it uses few trainable parameters and maintains the spatial configuration of the feature maps, as required for the attention step.

Multimodal Attention Module (MM-Att). The multimodal attention module is responsible for predicting attention at different spatial locations independently for appearance and semantic input streams. The spatial attention allows our network to selectively focus on discriminative and stable visual elements such as buildings instead of confusing/dynamic elements such as cars/pedestrians [5]. This results in embeddings that are more robust to perceptual changes especially in urban environments. We use the combined multimodal representation, computed by the fusion module, to sequentially predict a shared channel attention (denoted by  $\mathbf{M}_{c} \in \mathbb{R}^{C}$ ) and individual spatial attentions for the two modalities (denoted by  $\mathbf{M}_{xy}^{A} \in \mathbb{R}^{H \times W}$  and  $\mathbf{M}_{xy}^{S} \in \mathbb{R}^{H \times W}$  for appearance and semantic channels respectively). We believe that a tied channel attention allows sharing of information between the two modalities leading to a better spatial attention (as also evident later in our results in §4). The channel attention is computed by summarizing the feature maps across the spatial dimensions by average ( $\mathbf{F}_{avg}^{M}$ ) and max ( $\mathbf{F}_{max}^{M}$ ) pooling, and passing them through a multi-layer perceptron (MLP) followed by an addition and a non-linearity:

$$\mathbf{M}_{c} = \sigma(\phi(\mathbf{F}_{\text{avg}}^{M}) + \phi(\mathbf{F}_{\text{max}}^{M})), \tag{2}$$

where  $\sigma$  denotes the sigmoid function,  $\phi$  denotes a two-layer MLP shared across the two pooled inputs. The refined multimodal representation with attended channels is computed as  $\hat{\pmb{F}}^M = \pmb{F} \odot \pmb{M}_c$ , where  $\odot$  denotes element-wise multiplication with appropriate broadcasting (copying) of attention values along the spatial dimension.

The refined image representation is then used to predict per modality spatial attentions by using two  $7 \times 7$  convolutional filters— $\mathbf{W}_A^2$  and  $\mathbf{W}_S^2$ —for appearance and semantic input streams, respectively.  $\hat{\mathbf{F}}^M$  is pooled across the channel dimension by both average ( $\hat{\mathbf{F}}_{avg}^M$ ) and max ( $\hat{\mathbf{F}}_{max}^M$ ) pooling and concatenated across the channel dimension and convolved with the corresponding filters. The spatial attention maps are then used with the common channel attention to attend to the transformed maps from Equation 1 and generate refined features denoted as  $\hat{\mathbf{F}}^A$  and  $\hat{\mathbf{F}}^S$  for  $App_{mid}$  and  $Sem_{high}$ , respectively:

$$M_{xy}^{Z} = \boldsymbol{M}_{c} \odot \sigma(\hat{\boldsymbol{W}}_{Z}^{2} \circledast ([\hat{\boldsymbol{F}}_{avg}^{M}; \hat{\boldsymbol{F}}_{max}^{M}])) \quad \forall Z \in \{A, S\}$$
(3)

The final attended features  $\hat{\boldsymbol{F}}^A$  and  $\hat{\boldsymbol{F}}^S$  from the appearance and semantic input streams are

Method	Semantic	Attention	Nordland Sum.→Win.	St. Lucia		RobotCar	
				Average	Worst	$AM{\rightarrow}PM$	Sum. $\rightarrow$ Win.
App [Baseline]			58.0	71.4	55.5	36.6	79.6
App+Sem	✓		74.6	74.9	60.6	61.4	87.9
App-Att		✓	74.2	74.0	60.3	60.9	86.5
App-Att+Sem-Att	✓	✓	68.5	73.9	58.9	62.9	83.6
SAANE [Proposed]	$\checkmark$	✓	77.3	78.3	69.1	67.3	88.5
DenseVLAD [15]			19.2	64.5	35.5	22.9	78.6
NetVLAD [■]			36.7	57.7	33.1	37.0	86.8
AMOSNet* [□]			45.6	75.3	63.7	45.3	75.1
APANet* [☎]		†	27.0	42.4	26.1	11.2	58.2
APANet-MM* [☎]	✓	†	24.9	41.2	23.0	16.4	58.3

Table 1: Evaluation results of the different models discussed in §4.2 and §4.4. We report area under the precision-recall curve (AUC) for each method. We show results with prior state-of-the-art models below the double line. \* denotes models that we implemented and trained on SPED dataset that was used to train our model. † denotes variants of spatial attention that are distinct from our proposed method.

given by  $\hat{\mathbf{F}}^A = \mathbf{F}_A^M \odot M_{xy}^A$  and  $\hat{\mathbf{F}}^S = \mathbf{F}_S^M \odot M_{xy}^S$  respectively. We use another modality fusion module to fuse these refined features and then input them to the spatial pooling module.

**Spatial Pooling Module.** This module is responsible for pooling the information from the attended and fused features from the previous modules. In this work we use spatial pyramid pooling (SPP) [ $\square$ ] since it has been previously shown to be effective, and does not include any trainable parameters. Other equally effective alternatives, such as NetVLAD [ $\square$ ], would work in our framework. Finally, following the intuition of Ranjan *et al.* [ $\square$ ], we  $L_2$ -normalize these embeddings and scale them by a factor of  $\alpha = 10$ .

**Loss.** We use a max-margin-based triplet ranking loss function to learn our model [17]. This loss optimizes the network such that images from similar locations should be located closer in the embedding space than images from different locations. For computational efficiency, we form triplets in an online manner by sampling them from each minibatch [17].

# 4 Experimental Results

We first describe our train/test datasets along with the evaluation metric (§4.1). We then compare our model against a strong DCNN baseline while carefully demonstrating the contribution of each component of our model (§4.2). Thereafter, we discuss qualitative results to provide important insights into the proposed attention module (§4.3). We finally compare our approach with state-of-the-art (SOTA) 2D-VL methods on the three test datasets (§4.4).

#### 4.1 Datasets and Evaluation

**Datasets.** We utilize a version of the Specific Places Dataset (SPED) [ $\square$ ] to train our model. We randomly sample  $\sim 2600$  cameras from the Archive of Many Outdoor Scenes [ $\square$ ] and download images collected every half hour from Feb-Aug 2014. We remove all images where (i) the camera feed was corrupted, obscured, or too dark for visibility, and (ii) capture location of the camera was not fixed. The final dataset comprises 1.3 million images drawn from 2079 cameras featuring significant scene diversity, ranging from urban roads to unpopulated landscapes, and appearance changes due to seasonal and day-night cycles. We train our model on this dataset and evaluate the performance on 2D-VL on three challenging datasets as

	#Frames		Appearance Variation			
Dataset	Database	Query	Viewpoint	Illumination	Weather	
Nordland [55]	1403	1403	None	Yes	Yes	
St. Lucia [🔼]	1409	$1350 \times 9^*$	Slight	Yes	No	
RobotCar [ <b>□</b> ] AM→PM	2210	2254	Slight	Yes	Slight	
RobotCar [➡] Sum.→Win.	2065	2408	Slight	Slight	Yes	

Table 2: A summary of the size of each of our test datasets and the variations they contain. (\* Following standard practice, results on the St. Lucia dataset are averaged over 9 different query sets from different times of day.)

shown in Table 2). Since our focus is long-term VL and not place recognition as mentioned previously, we use the benchmarks as described in [[, 50]]. For St. Lucia and Nordland, we use the procedure in [50] due to insufficient experimental details in [50]. Since the remaining datasets used in [50] were either less challenging (Eynsham) or small (Gardens Point), we adapt RobotCar [50] to provide a more challenging test-bed. We refer readers to §8 for additional details regarding the datasets.

Evaluation Metric. We report Area Under the Curve (AUC) by constructing precision-recall curves using "the ratio test" [ , 50]. In brief, a match between a query image and the database is considered positive if the ratio of the Euclidean distances of the best match and the second-best match by nearest neighbors is above some threshold. A positive match is a true positive if it is within 5 frames of the ground truth. A precision-recall curve is then constructed by varying the threshold on the ratio test. The use of the ratio test enables the measurement of the frame-by-frame matches without relying on the specific pose being made available, which is the case for our test datasets (collected as synchronized traversals of the same route). More concretely, as the ratio test requires the feature distance between the best and second-best match to be above some threshold, it actually provides a stricter requirement for correct localization than Recall@1 metric, which is used to evaluate place recognition.

Prior Methods. We refer readers to §7 for implementation details regarding our model. For a fair comparison with prior methods, we use the same backbone DCNN networks for all methods. We implement AMOSNet [ by fine-tuning all layers of the DCNN on the SPED dataset. We also implement a recent SOTA method using both attention and pyramid pooling: Attention-based Pyramid Aggregation Network (APANet) [ by first implement their proposed cascade pyramid attention block using the appearance features. Although their method did not utilize semantic information, we also experiment with a stronger counterpart that uses two cascade pyramid attention blocks over the multimodal feature maps as used in our work (plus our multimodal projection as in Equation 1). We use the learned attention to sum pool the spatial pyramid features across both modalities to achieve the final embedding. We also compare with implementations of DenseVLAD [ by and NetVLAD [ by I, trained on the Pitts30k visual place recognition dataset [ by I, provided by the respective authors.

## 4.2 Quantitative Results

The performance of the proposed method along with different baselines and prior SOTA approaches is presented in Table 1. We first compare our model with different baselines to

<sup>&</sup>lt;sup>2</sup>For Nordland, we use the synchronized frame correspondence. On the other test datasets, 5 frames covers the ground-truth frame variance (0–25 m), a stricter requirement for positive localization than is typically used for place recognition (25–40 m). See Appendix A for a detailed discussion.

highlight the benefits of the proposed ideas in using (i) *semantic* information, and (ii) novel *multimodal attention module* to focus on discriminative regions for visual localization.

We validate the benefits of semantic information by comparing the performance of the baseline model using only appearance information (App [Baseline]) with that using both appearance and semantic information (App+Sem). Across our test datasets, there is an average absolute improvement of 9%, with the largest gain (25%) on the RobotCar AM $\rightarrow$ PM by using semantic information.

The remaining variants (App-Att, App-Att+Sem-Att, and SAANE) serve to demonstrate the benefits of the proposed *attention* module. Between App [Baseline] and App-Att, we see an average performance hike of 8% (averaged on all datasets) from the attention module that learns to focus on informative visual regions. The improvements on Nordland (16%) from attention alone demonstrate the ability of the module to suppresses confusing regions. These consistent gains demonstrate the benefits of using spatial attention with appearance information. However, this does not seem to be the case if we naively compute attention for both modalities with separate attention modules and then combine the resulting features. For example, while comparing App-Att+Sem-Att—the model variant that predicts separate attention over each modality—with App+Sem, we observe only minor improvements on the RobotCar AM—PM dataset (2%), likely because there is no sharing of information between the two modalities to encourage semantically informed and more consistent attention maps.

Our model addresses this by using the fused multimodal image representation to predict spatial attention for each modality by first predicting an intermediate *shared channel attention*. SAANE yields the best performance across all variants on each dataset (12% improvement over the baseline and 4% over App+Sem and 5% over App-Att+Sem-Att). Both Nordland (9%) and St. Lucia (11% in the worst case) are further refined by sharing channel attention across modalities, while the most perceptually-challenging test, RobotCar AM $\rightarrow$ PM, sees a further performance increase of 4% over App-Att+Sem-Att and of 31% over App [Baseline]. The proposed model is thus able to show consistent improvements over different baselines across all datasets for the task of visual localization.

## 4.3 Qualitative Results

We show top retrievals in Figure 2 for a case with significant variations in viewing conditions. We visualize the attended regions by showing the spatial attention maps from both modalities along with the semantic segmentation maps. We show a query image from the Night Autumn matched against retrieved database images from the Overcast Autumn set of RobotCar (i.e., AM $\rightarrow$ PM in Table 1). For methods relying only on appearance information (i.e., AMOSNet and the baseline), the retrieved images in the rightmost column are incorrect but present similar scene layouts, while our model retrieves a match within two meters of the query location. We see that across time of day, the maps from both attention modalities remain consistent and focus on stable features, with the appearance attention focusing mostly on fine details such as lane markings or architectural elements and semantic attention giving emphasis to scene layout and skyline shape. Interestingly, we note the bus present in the matched database image, obscuring a significant part of the scene. While the appearance modality attends highly to the bus's features, as if it were any other structure, we can see that the semantic attention module has learned to disregard this region as a dynamic object and gives more emphasis to the remaining scene layout. These results show that the proposed attention module guides the features to look at consistent regions even across extreme changes in viewing conditions. We refer readers to ?? for further analysis on the semantic-classes of

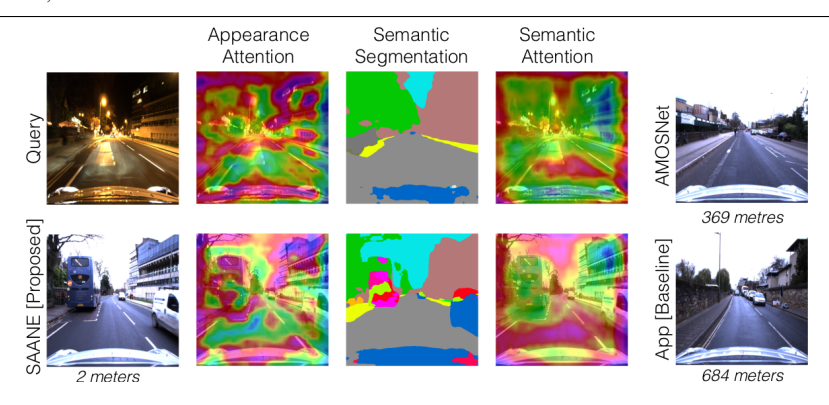


Figure 2: We present retrieval results under challenging appearance variations from RobotCar AM→PM to evaluate the quality of the our model and visualize the attention maps. We show a query image, database image retrieved using different methods, predicted attention maps, and the pre-computed semantic segmentation. The figure highlights that our model is able to retrieve the correct sample with and also produces attention maps that are consistent across extreme appearance changes. The palette for semantic segmentation is derived from ADE20K, as follows: skyscraper, sky, building, tree\_wall\_grass, sidewalk, car, plant, person\_earth, fence, signboard, pole, streetlight, truck\_conveyer, mountain, floor\_van. Figure best viewed in color.

regions attended across both modalities.

#### 4.4 Comparison with state-of-the-art

Table 1 shows the comparison of our model with several SOTA techniques. Our model shows consistent improvements on the test datasets in comparison to DenseVLAD (28% average absolute) and NetVLAD (19%), both SOTA 2D-VL methods. We note that NetVLAD performs comparably to our model on RobotCar Sum.  $\rightarrow$  Win, where the appearance changes are relatively minor; however, its performance is much lower on the test datasets with more extreme changes, which is consistent with prior work [211, 141]. We also observe an average absolute improvement of 12% (across all datasets) over AMOSNet, which was the previous SOTA method on both the Nordland and St. Lucia datasets. We note that for datasets which present minor appearance variation (e.g., St. Lucia), nearly the same result is achieved from fine-tuning on SPED (AMOSNet) as from adding additional semantic features (App+Sem). However, the capacity of our complete (SAANE) attention module to further refine the localization is shown again, with 3% improvement over AMOSNet. For cases with more severe appearance variation, we see a much larger improvement from training the proposed modules combining semantics, modality-specific spatial attention, and shared channel attention; e.g., results on the Nordland dataset show an absolute improvement of 32% and on RobotCar AM→PM an improvement of 22%. Similarly, SAANE also shows improvements between 37% and 38% over both implementations of APANet. Adding the semantic modality to APANet-MM is insufficient to significantly boost the performance of this pooling method in this scenario.

## 5 Conclusion

We present an attention-based, semantically-aware deep embedding model for image-based visual localization: SAANE. Our model targets the sensitivity of appearance-based visual localization to both perceptual aliasing from repetitive structures and extreme differences in viewing conditions. SAANE uses a novel multimodal attention module that fuses both mid-level appearance and high-level semantic features by predicting attention maps for both modalities with a shared channel attention. The attended maps are then fused to generate semantically informed image embedding. We evaluate the performance benefits of our model on three challenging public visual localization datasets, while showing significant gains compared to the baseline (12%) and prior state-of-the-art methods (19%). We also show that SAANE learns to produce stable attention maps that focus on consistent image regions across changing views, which is crucial for autonomous navigation.

# 6 Acknowledgement

We would like to thank Ajay Divakaran for proof-reading the manuscript and providing helpful comments.

#### References

- [1] Triantafyllos Afouras, Joon Son Chung, Andrew Senior, Oriol Vinyals, and Andrew Zisserman. Deep audio-visual speech recognition. *arXiv preprint arXiv:1809.02108*, 2018.
- [2] Karuna Ahuja, Karan Sikka, Anirban Roy, and Ajay Divakaran. Understanding visual ads by aligning symbols and objects using co-attention. *arXiv preprint arXiv:1807.01448*, 2018.
- [3] Peter Anderson, Xiaodong He, Chris Buehler, Damien Teney, Mark Johnson, Stephen Gould, and Lei Zhang. Bottom-up and top-down attention for image captioning and visual question answering. In *Proceedings of the IEEE Conference on Computer Vision and Pattern Recognition*, pages 6077–6086, 2018.
- [4] Asha Anoosheh, Torsten Sattler, Radu Timofte, Marc Pollefeys, and Luc Van Gool. Night-to-day image translation for retrieval-based localization. *arXiv preprint arXiv:1809.09767*, 2018.
- [5] Stanislaw Antol, Aishwarya Agrawal, Jiasen Lu, Margaret Mitchell, Dhruv Batra, C Lawrence Zitnick, and Devi Parikh. Vqa: Visual question answering. In *Proceedings of the IEEE international conference on computer vision*, pages 2425–2433, 2015.
- [6] Relja Arandjelović and Andrew Zisserman. DisLocation: Scalable descriptor distinctiveness for location recognition. In *ACCV*, pages 188–204, 2014.
- [7] Relja Arandjelović and Andrew Zisserman. Visual vocabulary with a semantic twist. In *ACCV*, pages 178–195, 2014.

- [8] Relja Arandjelovic, Petr Gronat, Akihiko Torii, Tomas Pajdla, and Josef Sivic. NetVLAD: CNN architecture for weakly supervised place recognition. In *CVPR*, pages 5297–5307, 2016.
- [9] Artem Babenko and Victor Lempitsky. Aggregating local deep features for image retrieval. In *ICCV*, pages 1269–1277, 2015.
- [10] Zetao Chen, Obadiah Lam, Adam Jacobson, and Michael Milford. Convolutional neural network-based place recognition. *arXiv preprint arXiv:1411.1509*, 2014.
- [11] Zetao Chen, Adam Jacobson, Niko Sünderhauf, Ben Upcroft, Lingqiao Liu, Chunhua Shen, Ian Reid, and Michael Milford. Deep learning features at scale for visual place recognition. In *ICRA*, pages 3223–3230, 2017.
- [12] Zetao Chen, Fabiola Maffra, Inkyu Sa, and Margarita Chli. Only look once, mining distinctive landmarks from convnet for visual place recognition. In *IROS*, pages 9–16, 2017.
- [13] Zetao Chen, Lingqiao Liu, Inkyu Sa, Zongyuan Ge, and Margarita Chli. Learning context flexible attention model for long-term visual place recognition. *IEEE Robotics and Automation Letters*, 3(4):4015–4022, 2018.
- [14] Girish Chowdhary, Eric N Johnson, Daniel Magree, Allen Wu, and Andy Shein. GPS-denied indoor and outdoor monocular vision aided navigation and control of unmanned aircraft. *Journal of Field Robotics*, 30(3):415–438, 2013.
- [15] Marius Cordts, Mohamed Omran, Sebastian Ramos, Timo Rehfeld, Markus Enzweiler, Rodrigo Benenson, Uwe Franke, Stefan Roth, and Bernt Schiele. The Cityscapes dataset for semantic urban scene understanding. In *CVPR*, 2016.
- [16] Mark Cummins and Paul Newman. FAB-MAP: Probabilistic localization and mapping in the space of appearance. *The International Journal of Robotics Research*, 27(6): 647–665, 2008.
- [17] Mark Cummins and Paul Newman. Appearance-only SLAM at large scale with FAB-MAP 2.0. *The International Journal of Robotics Research*, 30(9):1100–1123, 2011.
- [18] Chelsea Finn, Xin Yu Tan, Yan Duan, Trevor Darrell, Sergey Levine, and Pieter Abbeel. Deep spatial autoencoders for visuomotor learning. In *ICRA*, pages 512–519, 2016.
- [19] Akira Fukui, Dong Huk Park, Daylen Yang, Anna Rohrbach, Trevor Darrell, and Marcus Rohrbach. Multimodal compact bilinear pooling for visual question answering and visual grounding. *arXiv preprint arXiv:1606.01847*, 2016.
- [20] Sourav Garg, Niko Suenderhauf, and Michael Milford. LoST? appearance-invariant place recognition for opposite viewpoints using visual semantics. *Proceedings of Robotics: Science and Systems XIV*, 2018.
- [21] Ross Girshick. Fast R-CNN. In ICCV, pages 1440–1448, 2015.
- [22] Arren J Glover, William P Maddern, Michael J Milford, and Gordon F Wyeth. FAB-MAP + RatSLAM: Appearance-based SLAM for multiple times of day. In *ICRA*, pages 3507–3512, 2010.

- [23] Ruben Gomez-Ojeda, Manuel Lopez-Antequera, Nicolai Petkov, and Javier Gonzalez-Jimenez. Training a convolutional neural network for appearance-invariant place recognition. *arXiv* preprint arXiv:1505.07428, 2015.
- [24] Kaiming He, Xiangyu Zhang, Shaoqing Ren, and Jian Sun. Deep residual learning for image recognition. In *CVPR*, pages 770–778, 2016.
- [25] Arnold Irschara, Christopher Zach, Jan-Michael Frahm, and Horst Bischof. From structure-from-motion point clouds to fast location recognition. In *CVPR*, pages 2599–2606, 2009.
- [26] Nathan Jacobs, Nathaniel Roman, and Robert Pless. Consistent temporal variations in many outdoor scenes. In *CVPR*, pages 1–6, 2007.
- [27] Alex Kendall, Matthew Grimes, and Roberto Cipolla. PoseNet: A convolutional network for real-time 6-DOF camera relocalization. In *ICCV*, pages 2938–2946, 2015.
- [28] Diederik P Kingma and Jimmy Ba. Adam: A method for stochastic optimization. *arXiv* preprint arXiv:1412.6980, 2014.
- [29] Alex Krizhevsky, Ilya Sutskever, and Geoffrey E Hinton. Imagenet classification with deep convolutional neural networks. In *NIPS*, pages 1097–1105, 2012.
- [30] Svetlana Lazebnik, Cordelia Schmid, and Jean Ponce. Beyond bags of features: Spatial pyramid matching for recognizing natural scene categories. In *CVPR*, pages 2169–2178, 2006.
- [31] Yunpeng Li, Noah Snavely, Dan Huttenlocher, and Pascal Fua. Worldwide pose estimation using 3D point clouds. In *ECCV*, pages 15–29, 2012.
- [32] Hyon Lim, Sudipta N Sinha, Michael F Cohen, and Matthew Uyttendaele. Real-time image-based 6-DOF localization in large-scale environments. In *CVPR*, pages 1043–1050, 2012.
- [33] Stephanie Lowry, Michael Milford, and Gordon Wyeth. Transforming morning to afternoon using linear regression techniques. In *ICRA*, pages 3950–3955, 2014.
- [34] Jiasen Lu, Jianwei Yang, Dhruv Batra, and Devi Parikh. Hierarchical question-image coattention for visual question answering. In *Advances In Neural Information Processing Systems*, pages 289–297, 2016.
- [35] Will Maddern, Geoffrey Pascoe, Chris Linegar, and Paul Newman. 1 year, 1000 km: The Oxford RobotCar dataset. *The International Journal of Robotics Research*, 36(1): 3–15, 2017.
- [36] Michael J Milford and Gordon F Wyeth. SeqSLAM: Visual route-based navigation for sunny summer days and stormy winter nights. In *ICRA*, pages 1643–1649, 2012.
- [37] Tayyab Naseer, Luciano Spinello, Wolfram Burgard, and Cyrill Stachniss. Robust visual robot localization across seasons using network flows. In *AAAI*, pages 2564–2570, 2014.
- [38] Tayyab Naseer, Gabriel L Oliveira, Thomas Brox, and Wolfram Burgard. Semantics-aware visual localization under challenging perceptual conditions. In *ICRA*, pages 2614–2620, 2017.

- [39] Peer Neubert, Niko Sünderhauf, and Peter Protzel. Superpixel-based appearance change prediction for long-term navigation across seasons. *Robotics and Autonomous Systems*, 69:15–27, 2015.
- [40] Nathan Piasco, Désiré Sidibé, Cédric Demonceaux, and Valérie Gouet-Brunet. A survey on visual-based localization: On the benefit of heterogeneous data. *Pattern Recognition*, 74:90–109, 2018.
- [41] Noha Radwan, Abhinav Valada, and Wolfram Burgard. VLocNet++: Deep multitask learning for semantic visual localization and odometry. *arXiv preprint arXiv:1804.08366*, 2018.
- [42] Rajeev Ranjan, Carlos D Castillo, and Rama Chellappa. *L*<sub>2</sub>-constrained softmax loss for discriminative face verification. *arXiv preprint arXiv:1703.09507*, 2017.
- [43] Torsten Sattler, Michal Havlena, Filip Radenovic, Konrad Schindler, and Marc Pollefeys. Hyperpoints and fine vocabularies for large-scale location recognition. In *ICCV*, pages 2102–2110, 2015.
- [44] Torsten Sattler, Akihiko Torii, Josef Sivic, Marc Pollefeys, Hajime Taira, Masatoshi Okutomi, and Tomas Pajdla. Are large-scale 3D models really necessary for accurate visual localization? In *CVPR*, pages 6175–6184, 2017.
- [45] Torsten Sattler, Will Maddern, Carl Toft, Akihiko Torii, Lars Hammarstrand, Erik Stenborg, Daniel Safari, Masatoshi Okutomi, Marc Pollefeys, Josef Sivic, et al. Benchmarking 6DOF outdoor visual localization in changing conditions. In *CVPR*, 2018.
- [46] Johannes L Schönberger, Marc Pollefeys, Andreas Geiger, and Torsten Sattler. Semantic visual localization. In CVPR, 2018.
- [47] Florian Schroff, Dmitry Kalenichenko, and James Philbin. Facenet: A unified embedding for face recognition and clustering. In *CVPR*, pages 815–823, 2015.
- [48] Stephen Se, David Lowe, and Jim Little. Mobile robot localization and mapping with uncertainty using scale-invariant visual landmarks. *The international Journal of robotics Research*, 21(8):735–758, 2002.
- [49] Erik Stenborg, Carl Toft, and Lars Hammarstrand. Long-term visual localization using semantically segmented images. *arXiv preprint arXiv:1801.05269*, 2018.
- [50] Niko Sünderhauf, Sareh Shirazi, Feras Dayoub, Ben Upcroft, and Michael Milford. On the performance of convnet features for place recognition. In *IROS*, pages 4297–4304, 2015.
- [51] Linus Svärm, Olof Enqvist, Fredrik Kahl, and Magnus Oskarsson. City-scale localization for cameras with known vertical direction. *IEEE transactions on pattern analysis and machine intelligence*, 39(7):1455–1461, 2017.
- [52] Damien Teney, Peter Anderson, Xiaodong He, and Anton van den Hengel. Tips and tricks for visual question answering: Learnings from the 2017 challenge. In *Proceedings of the IEEE Conference on Computer Vision and Pattern Recognition*, pages 4223–4232, 2018.

- [53] Carl Toft, Carl Olsson, and Fredrik Kahl. Long-term 3d localization and pose from semantic labellings. In *Proceedings of the IEEE International Conference on Computer Vision*, pages 650–659, 2017.
- [54] Giorgos Tolias, Ronan Sicre, and Hervé Jégou. Particular object retrieval with integral max-pooling of CNN activations. *arXiv preprint arXiv:1511.05879*, 2015.
- [55] Akihiko Torii, Josef Sivic, Tomas Pajdla, and Masatoshi Okutomi. Visual place recognition with repetitive structures. In *CVPR*, pages 883–890, 2013.
- [56] Akihiko Torii, Relja Arandjelovic, Josef Sivic, Masatoshi Okutomi, and Tomas Pajdla. 24/7 place recognition by view synthesis. In *CVPR*, pages 1808–1817, 2015.
- [57] Sanghyun Woo, Jongchan Park, Joon-Young Lee, and In So Kweon. CBAM: Convolutional block attention module. In *ECCV*, 2018.
- [58] Chao-Yuan Wu, R Manmatha, Alexander J Smola, and Philipp Krähenbühl. Sampling matters in deep embedding learning. In *ICCV*, 2017.
- [59] Huijuan Xu and Kate Saenko. Ask, attend and answer: Exploring question-guided spatial attention for visual question answering. In *ECCV*, pages 451–466, 2016.
- [60] Zichao Yang, Xiaodong He, Jianfeng Gao, Li Deng, and Alex Smola. Stacked attention networks for image question answering. In *CVPR*, pages 21–29, 2016.
- [61] Joe Yue-Hei Ng, Fan Yang, and Larry S Davis. Exploiting local features from deep networks for image retrieval. In *CVPR workshops*, pages 53–61, 2015.
- [62] Bernhard Zeisl, Torsten Sattler, and Marc Pollefeys. Camera pose voting for large-scale image-based localization. In *ICCV*, pages 2704–2712, 2015.
- [63] Hengshuang Zhao, Jianping Shi, Xiaojuan Qi, Xiaogang Wang, and Jiaya Jia. Pyramid scene parsing network. In *CVPR*, pages 2881–2890, 2017.
- [64] Bolei Zhou, Hang Zhao, Xavier Puig, Sanja Fidler, Adela Barriuso, and Antonio Torralba. Scene parsing through ADE20K dataset. In *CVPR*, 2017.
- [65] Yingying Zhu, Jiong Wang, Lingxi Xie, and Liang Zheng. Attention-based pyramid aggregation network for visual place recognition. In *ACM MM*, pages 99–107, 2018.

# 7 Implementation Details

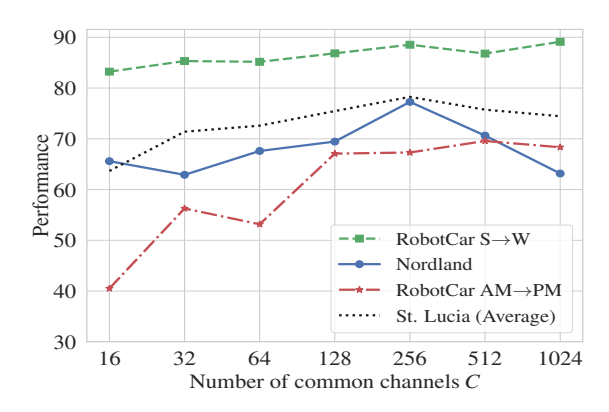


Figure 3: Figure shows a plot of performance of SAANE versus the number of channels C in the common multimodal fusion space.

The backbone of SAANE is two parallel DCNNs. We use a ResNet50 [24] pre-trained for the Imagenet classification task for mid-level feature extraction and a Pyramid Scene Parsing Network (PSPNet) [☑] pre-trained on the ADE20K [☑] semantic segmentation task for extracting semantic features. We also experimented with a version of PSPNet pre-trained on Cityscapes [12]; however, we found the ADE20K version to be more robust to viewpoint changes and the 150 classes of ADE20K to be more useful in the presence of diverse scene types. We use the output of the third residual block from ResNet50 as mid-level appearance features ( $\mathbf{F}^A$ ). For high-level semantic features ( $\mathbf{F}^S$ ), we use the output before the final convolutional layer of PSPNet. The resulting number of channels in appearance and semantic features are  $C_R = 1024$  and  $C_S = 512$ , respectively. We set the number of channels of the common embedding space in the modality fusion module (C), both before and after MM-Att, to 256. We use spatial pyramid pooling with pooling sizes of [4,3,2,1] and concatenate the feature maps from all layers to produce the final embedding. The dimensionality of the final embeddings after spatial pooling is 7680. For our experiments, we the two pre-trained DCNNs and fine-tune the two modality fusion modules and the MM-Att module. We use the Adam optimizer [22] with a learning rate of  $5 \times 10^{-5}$  and weight decay of  $5 \times 10^{-4}$  for training. We use online triplet sampling with batches comprised of 16 different classes with 4 examples per class. Within a batch, we utilize distance-weighted triplet sampling [☑] to increase the stability of the training process. We use a margin of m = 0.5, selected based on giving the best performance on a small validation set. Due to our assumption that our test data come from a dissimilar distribution as our training data, we did not by default experiment with any form of whitening as used in [8, 5].

Finally, to explore the effect of the model capacity on performance on the test datasets, we experiment with varying the dimensionality C of the multimodal fusion network. As shown in Figure 3, the performance across all of the datasets plateaus between 128 and 256 channels and shows evidence of overfitting, particularly in the case of Nordland, above 256 channels. The best dimensionality of the multimodal fusion module also appears to be a function of the dataset difficulty. Our model's performance on RobotCar Sum.  $\rightarrow$  Win., in the presence of minor seasonal variations, is relatively stable, even down to 16 channels, while the tasks with

more extreme variation, such as RobotCar AM → PM, sharply decline below 128.

#### 8 Test Datasets

Nordland [59] is derived from continuous video footage of a train journey recorded for a Norwegian television program, recorded from the front car of the train across four different seasons. We extract one frame per second from the first hour of each traversal, excluding images where the train is either stopped or in tunnels. This results in 1403 frames per traversal. We perform our experiments by constructing a database with the summer traversal and querying it with the winter traversal (Sum.—Win.). The images feature no viewpoint variation, due to travel on fixed rails; however, the seasonal appearance changes are quite severe.

**St. Lucia** [22] comprises ten different traversals recorded by a forward-facing webcam affixed to the roof of a car, following a single route through the suburb of St. Lucia, Queensland, Australia. This dataset was captured at five different times of day on different days across two weeks. We use the first traversal ('100909\_0845') as the database and query with the remaining nine, reporting the average as well as the worst case result over the nine trials. We sample images at one frame per second, which results in each traversal containing on an average 1350 frames. The dataset features slight viewpoint variations due to differences in the route taken by the vehicle. There are mild to moderate appearance changes due to differences in time of day and the presence of dynamic objects in the scene.

Oxford RobotCar [53] comprises several different traversals of the city of Oxford by a vehicle. It was collected across varying weather conditions, seasons, and times of day over a period of a year. We select two pairs of traversals, referred to as Overcast Autumn/Night Autumn and Overcast Summer/Snow Winter.<sup>3</sup> We perform an experiment by building a database with either Overcast Summer or Overcast Autumn and querying it with Snow Winter (Sum. → Win.) or Night Autumn (AM → PM), respectively. We make use of the center image from the front-facing camera and extract one frame per second. On average, each traversal covers nearly 9 km and 2000 frames. There are mild viewpoint variations present, again due to slight differences in the starting point and road position of the traversals. The appearance change in the day-night pair is quite drastic, largely from the difference in illumination quality in the transition from sunlight to street lights; while it is more moderate in the summer-winter pair, with minor variation from seasonal vegetation and ground cover.

<sup>&</sup>lt;sup>3</sup>The first three were introduced in [☑], and the traversals were originally referred to in [☑] as 2014-12-09-13-21-02, 2014-12-10-18-10-50, 2015-05-19-14-06-38, and 2015-02-03-08-45-10, respectively.